Journal of Power Sources 247 (2014) 1018–1025

Contents lists available at SciVerse ScienceDirect

Journal of Power Sources

journal homepage: www.elsevier.com/locate/jpowsour

The effect of thermal gradients on the performance of lithium-ion batteries

Yannic Troxler [a], Billy Wu [a,b], Monica Marinescu [b], Vladimir Yufit [b], Yatish Patel [a], Andrew J. Marquis [a], Nigel P. Brandon [b], Gregory J. Offer [a,*]

[a] Department of Mechanical Engineering, Imperial College London, UK
[b] Department of Earth Science and Engineering, Imperial College London, UK

HIGHLIGHTS

- Peltier element thermal tests under isothermal and non-isothermal conditions.
- Isothermal testing showing Arrhenius rate law for charge transfer resistance.
- Isothermal cycling to determine entropy vs SOC, compared to cyclic voltammetry.
- Electrochemical impedance under thermal gradients different to isothermal.
- Good fit of thermal gradients to model of discretized temperature dependent nodes.

ARTICLE INFO

Article history:
Received 5 March 2013
Received in revised form
2 June 2013
Accepted 12 June 2013
Available online 25 June 2013

Keywords:
Lithium-ion battery
Thermal testing
Thermal modelling
Thermal gradients
Entropy measurements

ABSTRACT

An experimental apparatus is described, in which Peltier elements are used for thermal control of lithium-ion cells under isothermal and non-isothermal conditions, i.e. to induce and maintain thermal gradients. Lithium-ion battery packs for automotive applications consist of hundreds of cells, and depending on the pack architecture, individual cells may experience non-uniform thermal boundary conditions. This paper presents the first study of the impact of artificially induced thermal gradients on cell performance.

The charge transfer resistance of a 4.8 Ah is verified to have a strong temperature dependence following the Arrhenius law. Thermal cycling of the cell, combined with slow rate cyclic voltammetry, allows to rapidly identify phase transitions in electrodes, due to the thermal effect of entropy changes. A cell with a temperature gradient maintained across is found to have a lower impedance than one held at the theoretical average temperature. This feature is attributed to details of the inner structure of the cell, and to the non-linear temperature dependence of the charge transfer resistance.

1. Introduction

In recent years, the Li-ion battery has emerged as the technology of choice for electric vehicles due to its relatively high energy and power density [1]. Because safety and performance are the major challenges faced today, the thermal control of Li-ion cells becomes crucial. One of the main concerns is the heat generated within the cell, which may cause the onset of thermal runaway [2–4]. The study of the ageing and degradation of individual cells [5,6] and of their response to abuse [7] is intrinsically related to thermal effects. In recent years, this subject has received much interest, with many studies analysing the effect of temperature on Li-ion cells [2,4,6–19].

In order to achieve practical voltage and capacity values for hybrid and electric vehicles, a large number of cells are connected in series and parallel to form the battery pack. As such vehicles enter mass production, developers must understand the ageing modes and predict the lifetime of battery packs. Despite this need, relatively few studies in the literature address cell behaviour under the impact of battery pack design and integration [18,20–23]. In most cases, inhomogeneity's within individual cells are ignored during pack modelling [21,23], and coupled multi-dimensional electro-thermal models are normally only deployed at the cell level [16,20]. As a result, the impact of thermal gradients across a cell caused by pack design is rarely considered, although they are expected to arise [18].

* Corresponding author.
E-mail address: gregory.offer@imperial.ac.uk (G.J. Offer).

0378-7753/$ – see front matter © 2013 Elsevier B.V. All rights reserved.
http://dx.doi.org/10.1016/j.jpowsour.2013.06.084

Early reviews report that Li-ion cell performance, in particular capacity fade, is sensitive to the operating temperature [7,10,19]. Bandhauer et al. [10] showed that power and capacity can degrade significantly when cells are operated or stored at temperatures above 50 °C and at high States Of Charge (SOCs). The same trend was reported by Spotnitz et al. [7], who described various failure modes and consequences of thermal runaway, such as the breakdown of the Solid Electrolyte Interphase (SEI) at temperatures above 90 °C, leading to the degradation and even abrupt failure of the cell. Vetter et al. [6] reported that high temperatures accelerate capacity fade, but low temperatures, especially during charging, are also detrimental, as they lead to lithium plating and dendrite growth.

Cell behaviour is commonly characterised by a technique known as Electrochemical Impedance Spectroscopy (EIS) [14,24]: the phase and magnitude of the voltage/current response are measured for an applied low amplitude sinusoidal current/voltage. By varying the frequency of the input, the occurrence of different processes in the cell can be identified by fitting the response to an equivalent circuit model [25]. The impedance characteristics of Li-ion batteries are well studied, including the effect of SOC [12,19,20,26,27], temperature [9,25,28,29], or both on the cell performance.

A more recent technique called electro-thermal impedance spectroscopy has been developed by Schmidt et al. [30], building upon earlier work by Barsoukov et al. [31] and Forgez et al. [24]. They applied a 17 kHz oscillating current to heat up the cell; changes in the surface temperature are measured to calculate the thermal impedance of the cell and parameterise thermal models. Nagpure et al. [32] investigated cathode degradation with the help of a flash heating lamp and a thermal imaging camera used to measure the thermal conductivity of a Li-ion cell. Hensler et al. [33] applied a similar technique to Schmidt et al. at pack level.

The standard equivalent circuit model for one cell has fixed-value parameters, but dependence on SOC, temperature, and current are often needed for realistic modelling. Eddahech et al. [34] used EIS data and an equivalent circuit model to show that SOC, temperature and number of cycles are dominant factors for SEI-layer growth and cell ageing. However, Chaturvedi et al. [35] note that the model requires large number of parameters to mimic the complex electrochemical behaviour of the battery.

Although the performance of a Li-ion cell is known to be strongly dependent on temperature, battery suppliers and manufacturers seldom provide the temperature dependent characteristics of a cell. In response to this need, various methods to control and monitor thermal conditions have been investigated. Resistive heating bands wound around cylindrical cells [31], thermal imaging cameras [32,36], and embedded thermocouples [24] have all been used. Most groups, however, use multiple external thermocouples for surface measurements, and climate chambers [24,25,37,38] to fix the temperature across the cell. These can be simple devices such as a refrigerator/oven controlled by a thermostat, or complex ones, such as those offered by Weiss, which comprise of a sealed compartment that can be flooded with inert gas [39]. Yazami et al. [40] maintained the temperature inside the climate chamber using Peltier elements instead of a refrigeration pump. When heating through convection, the cell takes a long time to reach thermal equilibrium. More importantly, such devices are not able to impose thermal gradients across the cell.

Relatively few studies have investigated the effects of thermal gradients. Battery packs and cells have been modelled in 3D to study the temperature gradients arising within them [16,18,41]. More recently, Fleckenstein et al. [15] found that temperature gradients can induce localised fast ageing, resulting in accelerated ageing of the cell compared to its behaviour under homogeneous temperature distribution. Kim et al. [17] found that the variation of potential across current collectors and of temperature across the cell can impact battery response.

Accurately predicting the thermal behaviour of Li-ion batteries under realistic conditions is important for improving performance, safety and cell longevity. During aggressive charge/discharge cycles for the large form factor cells used in EVs and HEVs applications, temperature gradients cannot be ignored. This study reports a test rig capable of controlling and monitoring the temperature on the different surfaces of a Li-ion battery by using heat conduction. The rig is used for a series of tests that investigate the effect of thermal gradients on battery impedance at various SOCs and temperatures, as well as entropy effects at the different SOCs. All tests are performed on a 4.8 Ah Kokam Li-ion polymer cell.

2. Design and experimental setup

2.1. Safety and materials

Fig. 1 depicts the thermal testing rig: compartment A contains the cell, compartment B contains the electronic components and is isolated to protect the electronics in the event of a battery failure. The walls of the rig are made of Polycarbonate (PC) due to its high impact and fire resistance, and are transparent for visibility. The cell itself and an adjustable cell holder are mounted onto a removable insulated ground plate in compartment A, as shown in Fig. 2. This modular design allows a broader use of the rig: cell holders for different cell sizes and geometries can be added.

2.2. Heating and cooling

Thermoelectric cooler elements impose the thermal boundary conditions on the cell. Each element consists of two ceramic plates with a P–N-type semiconductor array in-between. Upon applying a voltage across the plates, heat is transferred from one side of the semiconductor to the other at a rate that is dependent on the current supplied; this is known as the Peltier effect and the elements are referred to as Peltier elements (PEs). The PEs can be used for either cooling or heating, depending on the direction of the current flow. The PEs are in contact with the two opposite sides of the cell, such that the cell itself is cooled/heated, while the compartment remains at ambient temperature. In this setup, both isothermal and thermal gradient tests can be performed.

In general, PEs have low efficiencies, especially if a large amount of heat and therefore large temperature gradient is required. A heat sink that reduces the thermal gradient across each PE is therefore included in the form of recirculating water placed outside the main compartment. The heat sink is connected to side of the PE opposite from that in contact with the cell, as depicted in Fig. 3. As the PE does not cover the entire cell surface, copper plates are inserted

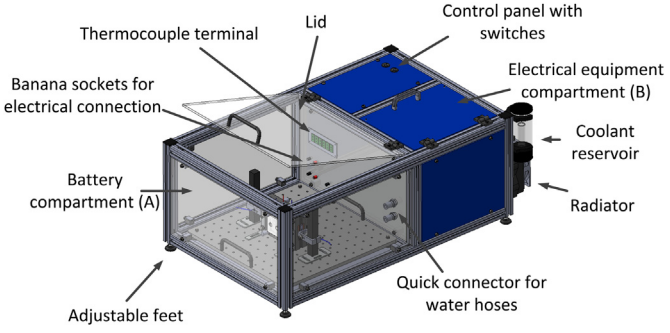

Fig. 1. Rig for thermal testing of battery cells.

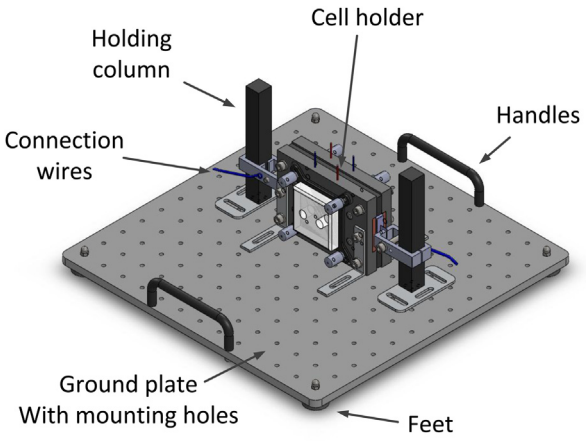

Fig. 2. Removable cell holder and ground plate in compartment A.

between the PEs and the cell surface to ensure a homogeneous temperature distribution. Copper was chosen for its high thermal conductivity and diffusivity. Thermal simulation predictions in SolidWorks indicate that in the worst case scenario of the PE being cooled to −15 °C and natural convection occurring on any uninsulated sides of the cell, a difference of 1.5 °C is established between the centre and the edges of the copper plate.

In order to minimise the thermal contact resistance between the PE, heat sink and copper plate, a thin layer of silicon free graphite based heat transfer compound (10.5 W mK^{-1}) was used to fill any gaps between the uneven contact surfaces. Although much higher than that of air, the thermal conductivity of this compound is significantly lower than that of copper.

3. Measurement procedures

For experiments varying temperature, the cell was equilibrated for 30 min; doubling the time did not change the results. For experiments varying SOC, the cell was equilibrated for at least 12 h.

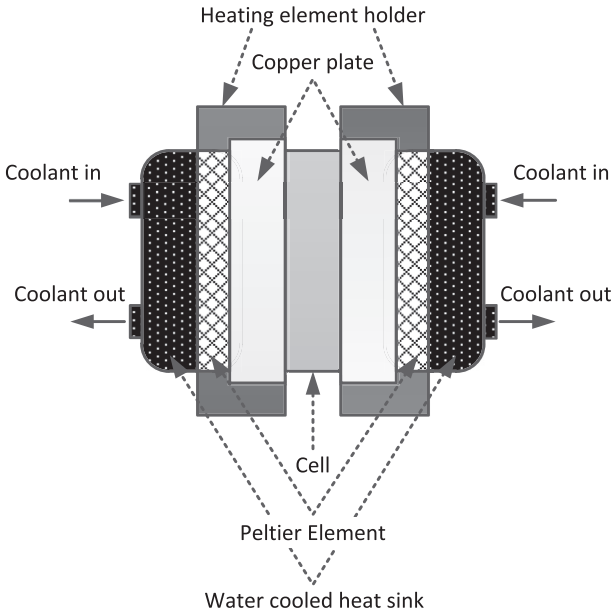

Fig. 3. Cell holder, with Peltier elements and heat sink connections.

3.1. Temperature controls

A PicoLog TC-08 data logger collects temperature data from the type-K thermocouples at the centre and ends of the cell, as well as the ambient temperature and that of the cooling fluid. Cold junction compensation is integrated into the device. Two Agilent 3632A power supplies (rated at 120 W) power the PEs. By using an array of relays, both positive and negative voltages are applied to the PEs, allowing them to either heat or cool the cell. Each heat pump is connected to a PID controller programmed in LabView.

3.2. Constant current measurements

The voltage of the cell is measured by an Agilent 34970A data acquisition unit with input impedance >10 MΩ, and maximum resolution ≈ 10 μV. A constant low current discharge test from 100% SOC (4.2 V) for the Kokam cell was used to define the voltage vs SOC relationship at ambient temperature, by integrating the current. Prior to testing, the cell was saturated in constant voltage mode at 4.2 V until the charging current dropped to below 20 mA. Fig. 4 shows the obtained discharge curve with cut-off potential of 2.7 V. Under the lowest discharge current of 1.2 A, the capacity of the cell is 4.63 Ah. This value represents a 3% decrease on the manufacturers rated 4.8 Ah, unsurprising since the cell was two years old.

Both temperature and SOC affect the values of the Open Circuit Voltage (OCV). The time required for cells to equilibrate after charging/discharging, however, is expected to be considerably longer than that required for temperature equilibration, because the characteristic time for the thermal inertia is shorter than that of diffusion of lithium through the solid electrode phase.

3.3. EIS measurements and data fitting

EIS measurements were performed by a potentiostat/galvanostat (Autolab PGSTAT30) with a 10 A current booster (Autolab BSTR10A), controlled via the Nova (version 1.6) software. The performance of the Kokam 4.8 Ah cell was investigated in a frequency range 0.1 Hz to 5–10 kHz, covering most of its performance spectrum. Detecting the purely diffusive behaviour requires long-duration measurements down to 0.01 Hz, which were too noisy and not the main focus of this work. An input current amplitude of 0.2 A RMS was chosen. This value is low enough to ensure operation at constant SOC and to maintain the system within a linear regime,

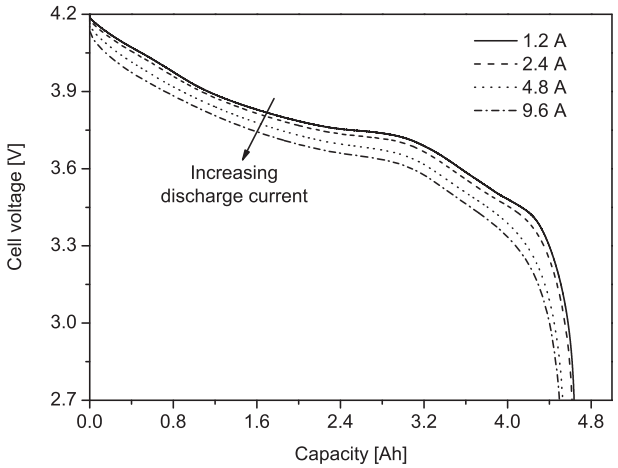

Fig. 4. The available cell capacity varies with the value of discharge current. Discharge curves for a 4.8 Ah Kokam Li-ion polymer cell at ambient temperature.

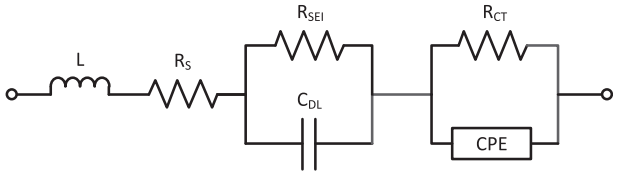

Fig. 5. The equivalent circuit used to analyse the EIS data.

while high enough to ensure a good signal-to-noise ratio. The ZView (Scribner) software was used to fit the EIS data to the equivalent circuit in Fig. 5 via a Levenberg–Marquardt complex non-linear least-square algorithm.

The circuit consists of four blocks, representing the various processes taking place inside the cell [42]. The inductance L captures the behaviour at very high frequencies, where the inductance in the wiring of the experimental setup and that of the cell dominate. R_S is the series resistance of the cell, attributed to the electronic and ionic resistances of the battery materials, current collector–electrode interfaces, and contacts. Lithium transport through the SEI-layer is represented by a parallel RC circuit. The charge transfer mechanism allowing intercalation/deintercalation of the Li-ions is represented by a resistor in parallel with a Constant Phase Element (CPE). A Warburg element was not included, as the frequency range is kept below the level at which solid state diffusion effects dominate.

4. Results and discussion

4.1. Rig validation

EIS data was recorded and analysed in order to explore the rig capabilities. Fig. 6 shows the EIS spectra obtained from the 4.8 Ah Kokam Li-ion polymer cell tested at 15 °C and different SOCs. The dominant process is the charge transfer resistance (R_{CT}), identifiable by the radius of the large depressed semicircle. The fitted R_{CT} values vary exponentially with SOC, as shown in Fig. 7: the lower the cell voltage, the higher the cell impedance. The reduced performance at low SOCs is caused by low rate extraction of metallic lithium from the graphite anode at low stoichiometries.

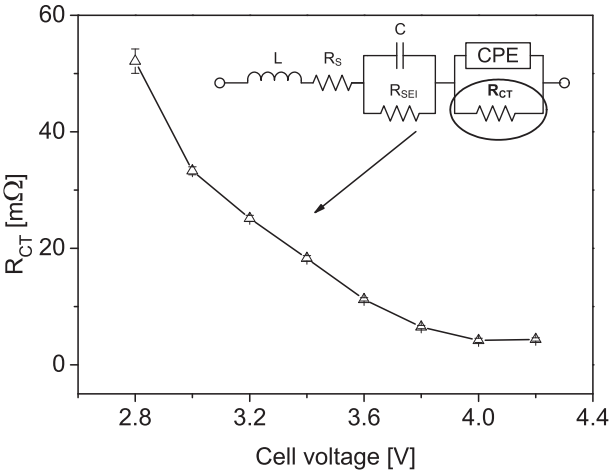

Fig. 7. Charge transfer resistance of a 4.8 Ah Kokam Li-ion polymer cell at 15 °C and different SOC values (error bars included, but very small).

The dependence of cell behaviour on applied surface temperature was investigated between −13 °C and 55 °C, corresponding to the lowest temperature achieved by the rig, and 5 °C below the recommended upper limit of the operating range (60 °C). The EIS spectra for this temperature range at 50% SOC are shown in Fig. 8. Fig. 9 displays the variation of fitted R_s and R_{CT} with temperature.

Both R_s and R_{CT} decrease exponentially with increasing temperature, following the Arrhenius law. This dependence indicates the ionic conductivity of the electrolyte as the major contribution to R_s. R_{CT} dominates the cell impedance at low to medium temperatures and its temperature dependence: at −13 °C R_{CT} is about 90 times higher than R_s, and it decreases 250 times between −13 °C and 55 °C. The R_{CT} dependence on temperature can be fitted with the Arrhenius law in Equation (1).

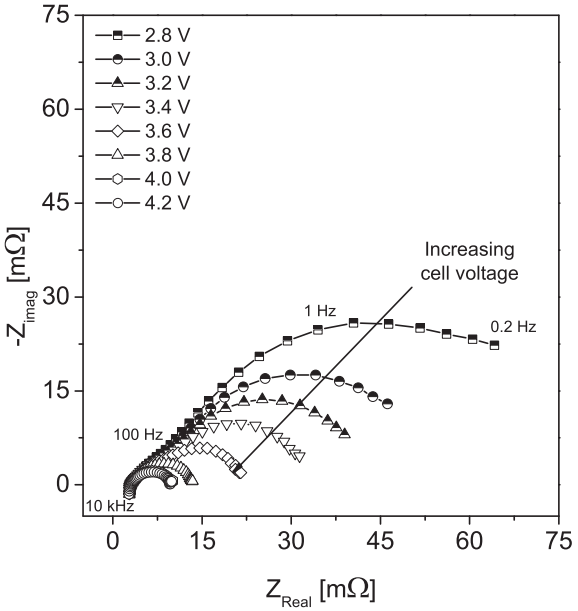

Fig. 6. The impedance of the cell decreases with increasing SOC. EIS spectra of a 4.8 Ah Kokam Li-ion polymer cell at 15 °C for various SOC values.

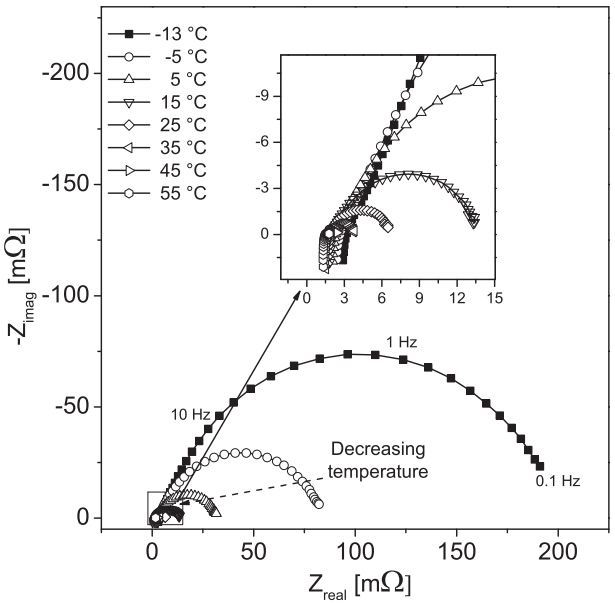

Fig. 8. EIS spectra of a 4.8 Ah Kokam Li-ion polymer cell at 50% SOC at different temperatures.

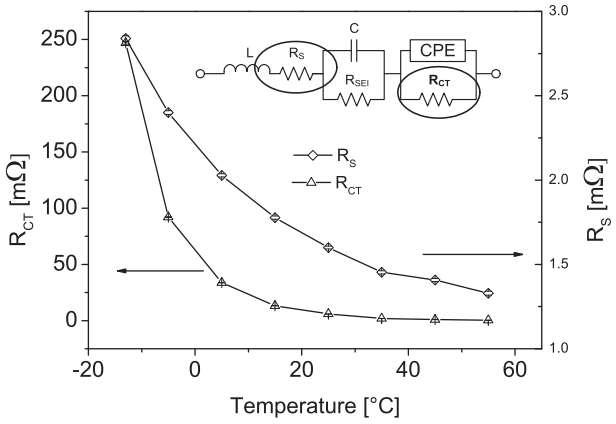

Fig. 9. Temperature dependence of fitted charge transfer and series resistances of a 4.8 Ah Kokam Li-ion polymer cell at 50% SOC (error bars included, but very small).

$$R_{CT} = R_{CT,ref}\exp\left(\frac{E_a}{R}\left(\frac{1}{T}-\frac{1}{T_{ref}}\right)\right) \quad (1)$$

R_{CT} is the charge transfer resistance (Ω), $R_{CT,ref}$ the charge transfer resistance at the reference temperature (Ω), E_a the activation energy (J mol^{-1}), R the universal gas constant (J mol^{-1} K^{-1}), T the temperature (K), and T_{ref} the reference temperature (K); here T_{ref} = 298.15 K. The fit agrees well with experimental data at 50% SOC, yielding a coefficient of determination R^2 = 0.999 for E_a = 65.47 kJ mol^{-1}.

4.2. Entropy effects

The OCV of a Li-ion cell varies with temperature as a result of entropy changes (ΔS) in the two electrodes. The sign of ΔS varies with SOCs [40]. Accurate models of the thermal behaviour of Li-ion cells must include information on the entropy changes.

To quantify the temperature dependence of OCV, the Kokam cell was thermally cycled from 25 °C to 55 °C, down to −13 °C and then back to 25 °C in 10 °C steps. The rate of change of voltage with respect to temperature (dV_{OC}/dT^{-1}) indicates entropy changes in the cell at the given SOCs. Fig. 10 displays the data obtained for 9% SOC. The measured OCV responds almost instantaneously to changes in imposed temperature.

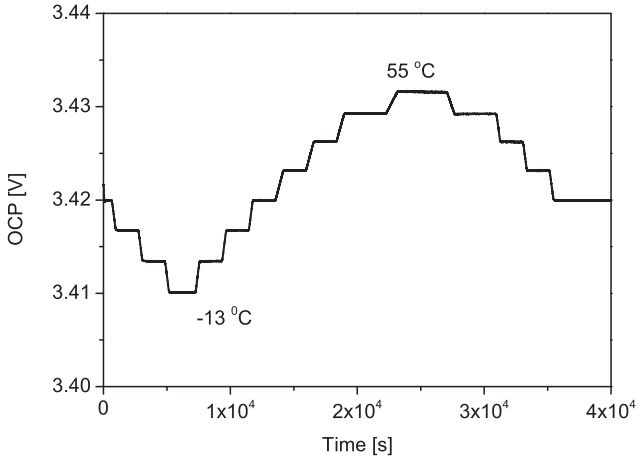

Fig. 10. OCV as a result of surface temperature cycling. The cell has been equilibrated overnight at 9% SOC. The temperature was varied between −13 °C and 55 °C in 10° increments.

Similar measurements were performed at various SOCs. In every case the OCV is found to vary linearly with temperature, as previously found by Kumaresan et al. [43] and Ye et al. [44], allowing the fit in Equation (2):

$$V = V_{ref} + \left(T - T_{ref}\right)\frac{\partial V_{OC}}{\partial T} \quad (2)$$

V_{ref} is the OCV value at T_{ref} = 25 °C. The term $\partial Voc/\partial T$ is a measure of the reversible heat generation Q_{rev} or entropy changes ΔS in the cell [40], as given in Equation (3).

$$\dot{Q}_{rev} = IT\frac{\partial Voc}{\partial T} = IT\frac{\Delta S}{nF} \quad (3)$$

I [A m^{-1}] is the current density, n = 1 the charge number for Li-ions, and F [C mol^{-1}] the Faraday constant. The values of $\partial V_{OC}/\partial T$ at various OCVs, corresponding to entropy changes, are plotted as symbols in Fig. 11. This data should be useful in inferring the composition of the cell cathode. Saito et al. [45] show that a phase transition between 0 and 20 %DOD or 100 and 80% SOC corresponds to $LiCoO_2$ hexagonal to monoclinic crystallographic phase transformation. In the current study there is no data available between 4.0 and 4.2 V and therefore the composition of the cathode cannot be established.

The entropy information is compared with slow scan cyclic voltammetry (SSCV) data during charging at a sweep rate of 10 μV s^{-1}, plotted vs. the apparent OCV, i.e. the average cell potential during charge and discharge. As indicated by Fig. 11, for the cell used, the positions of the positive and negative peaks associated with entropy changes correspond to similar features in the SSCV. Therefore, either technique can be used to detect phase transitions occurring at anode and cathode electrodes during battery operation [40,46]. It should be noted that this correlation between SSCV peaks and dV_{OC}/dT^{-1} data is not always valid. For example, in the case of LiFePO4 cathodes, the dV_{OC}/dT^{-1} curve is flat over a wide range of SOCs, between 10% and 90% [47].

It is difficult, however, to decouple anode and cathode phase transition contributions to the cumulative measured entropy change when the information is gathered from full cell experiments. Moreover, these measurements are performed on commercial batteries, for which exact composition and crystallographic data on each electrode is not available. The technique presented here, however, can be used to measure entropy changes as a function of SOC, and use this information to parameterise thermal models to improve accuracy.

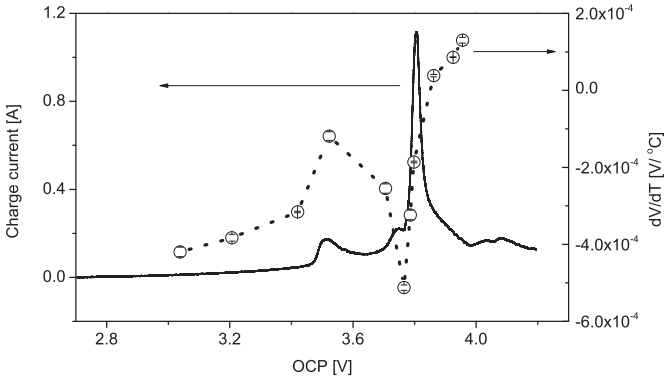

Fig. 11. $dV\,dT^{-1}$ at different SOCs for a 4.8 Ah Kokam Li-ion polymer cell, and slow rate cyclic voltammetry data for charging at a scan rate of 10 μV s^{-1}.

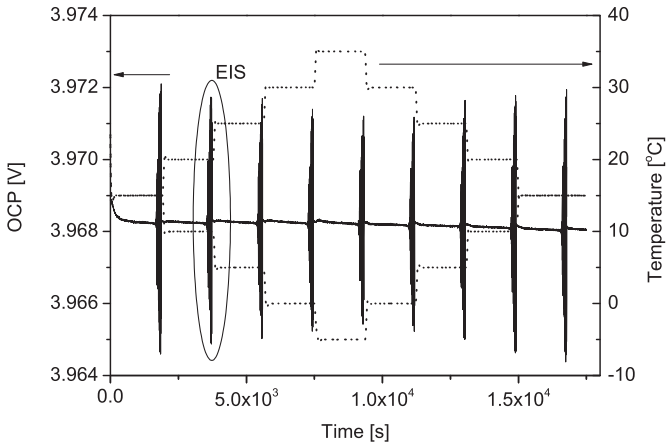

Fig. 12. OCV measurements for different applied thermal gradients at 80% SOC and fixed 15 °C average temperature.

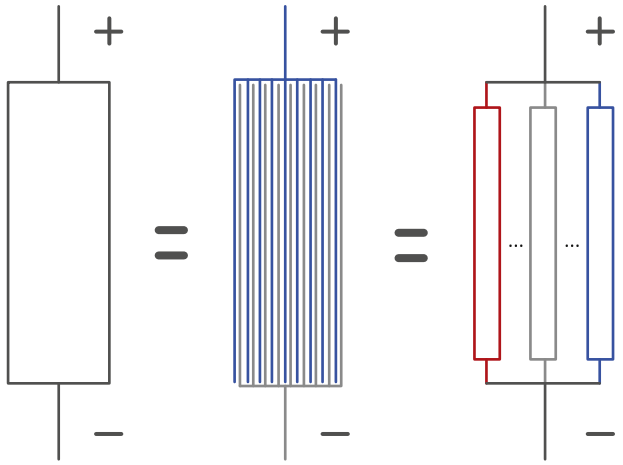

Fig. 14. Schematic of the internal structure of a 4.8 Ah Kokam Li-ion polymer cell.

4.3. Effects of temperature gradients

The presented rig allows control over imposed thermal gradients across a single cell, in order to study the performance under conditions similar to those experienced in a battery pack. A first characterisation of the effects of temperature gradients on cell performance is obtained from EIS spectra. At a fixed SOC and theoretical average temperature, one side of the cell is cooled and the other is heated, each in increments of 5 °C, to a maximum difference of 40 °C across the cell. Nine sets of measurements are taken: $T_{avg} = 15$ °C, 25 °C and 35 °C, and 20%, 50% and 80% SOC, each lasting approximately 5 h Fig. 12 displays the measured temperature at the centre of the cell surface and the corresponding OCV against time for a cell at 80% SOC and $T_{avg} = 15$ °C. The noise in the voltage measurements are a result of the EIS being performed, each 3–4 min long.

The nine EIS spectra are displayed on a Nyquist plot in Fig. 13. The presence of a temperature gradient decreases the cell impedance when compared to the isothermal impedance; the higher the gradient, the smaller the amplitude of the measured voltage response. The effect of temperature gradients is larger in the limit of low to medium frequencies, while at high frequencies the cell performs as at a uniform temperature T_{avg}. This observation is consistent with the temperature dependency presented in Fig. 9; the effect of thermal gradients on R_{CT} is larger than that on R_S. The trend in Fig. 13 is reproducible, as data obtained on the ascending branch of the temperature profile matches that on the decreasing branch within measurement error.

X-ray images taken by Yufit et al. [48] show the internal structure of the cell: a stack of ≈80 alternating anode-separator-cathode units, each of ≈100 μm thickness. Due to the comb-like structure, the cell is electrically equivalent to a parallel connection of the basic units. The thickness of each unit is small relative to that of the cell, such that the temperature can be assumed constant across one unit, but variable from one unit to the other [49], as shown schematically in Fig. 14. This simplification of a cell, together with the information collected from isothermal experiments, which showed that both R_{CT} and R_S decrease exponentially with temperature, enables one to interpret the effects of temperature gradients. The basic units located close to the hotter side have lower effective impedance, causing larger currents to pass through them than through the units close to the colder side. As a result, the performance of the cell is dominated by the properties of the hotter units, and the cell behaviour as a whole resembles that of a cell hotter than T_{avg}.

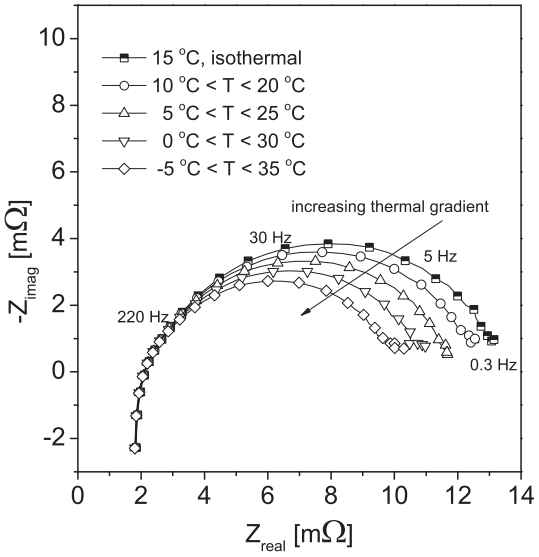

Fig. 13. The fitted curves are marked as a continuous lines and the measured data is shown with symbols. The isothermal data (no gradient) is marked in black $T_{avg} = 15$ °C and SOC = 50%.

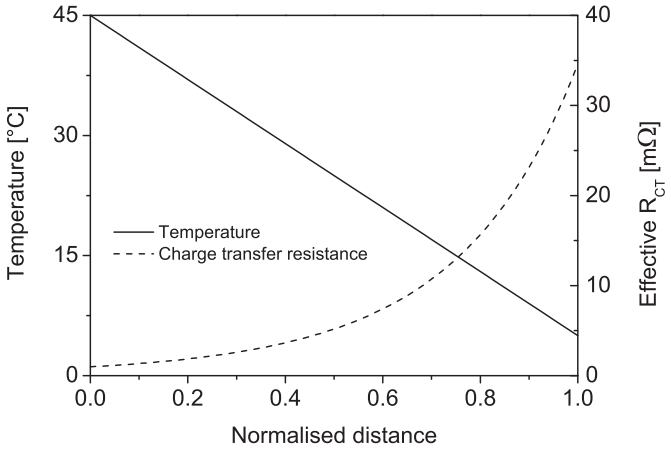

Fig. 15. Temperature profile across a cell and associated equivalent charge transfer resistance.

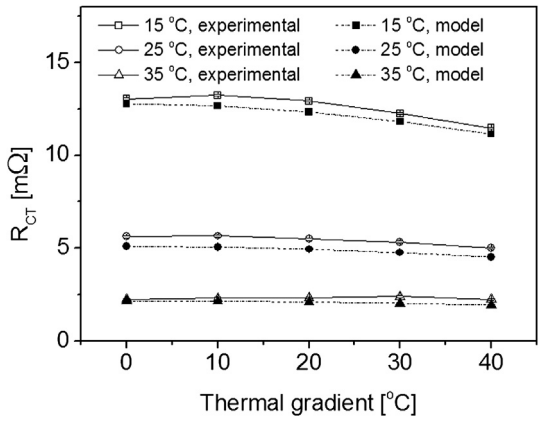

Fig. 16. Theoretical predictions and experimental data for the charge transfer resistance of a 4.8 Ah Kokam Li-ion polymer cell at 50% SOC, at different average temperatures and thermal gradients.

Assuming the imposed temperature gradient leads to a linear temperature variation across the 80 units in the cell, the R_{CT} of each unit can be calculated for the respective temperature, using the activation energy obtained in Equation (1) from fitting isothermal data. Fig. 15 displays the assumed temperature distribution across a cell and the resulting local equivalent R_{CT}.

The effective R_{CT} of the entire cell can be calculated as the parallel configuration of the resistor values obtained as detailed above. By using this method, it is possible to predict the effective R_{CT} for a cell at any given thermal gradient. Fig. 16 compares the predicted cell R_{CT} values with those fitted from experimental data for a 50% SOC, showing a good agreement, especially for the higher average temperatures. At lower temperatures, such as at $T_{avg} = 15$ °C, processes such as diffusion, not included in the equivalent circuit model, influence R_{CT}.

For relatively small T_{avg} values, R_{CT} decreases significantly with increasing temperature gradient. At higher T_{avg} values, there is little change in cell R_{CT} with temperature gradient. This trend is consistent with data shown in Fig. 9: the temperature variation of R_{CT} is stronger at lower temperatures. For the other parameters of the equivalent circuit, the observed variations due to temperature gradients were weaker. Combining this technique with a thermal model of a cell and surface temperature measurements could help determine core cell temperature from EIS measurements.

5. Conclusions

A test rig has been designed and built that rapidly and accurately controls the thermal boundary conditions of Li-ion cells using Peltier elements during electrical testing. Thermal gradients can be artificially induced and maintained across a single cell. Isothermal tests using this rig yield entropy trends similar to those previously documented, and are validated against slow scan cyclic voltammetry data. The measurements are sufficiently accurate to detect phase changes in either of battery electrodes.

Under temperature gradients, the cell was found to not perform as under a uniform temperature equal to the theoretical average temperature of the imposed gradient, but as a cell at a higher average temperature. The larger the gradient, the larger the deviation from the behaviour of a cell with a constant average temperature.

A simple model is capable to predict the cell effective charge transfer resistance for any imposed thermal gradient, without the need for thermal gradient experiments. The model is based on an equivalent circuit model of the cell, knowledge of its internal structure, assumption of Arrhenius law temperature dependence of charge transfer resistance, and linear temperature variation across the cell. The method follows these steps: the temperature dependent activation energy of the cell is extracted from isothermal measurements; the cell is conceptually decomposed into its 80 parallel anode-separator-cathode units, each with a discrete temperature value; the temperature profile across the pouch cell is set as linear; the effective charge transfer resistance of the cell under thermal gradient is composed of 80 parallel resistors with values calculated at their respective temperatures. There is a good agreement between model predictions and experimental data, especially for temperatures around room temperature and higher.

Cell behaviour was tested exclusively for zero load. It is expected that its performance is strongly affected by temperature gradients during charge/discharge, and that the corresponding average temperature is not a good indicator. Since the hotter part of the cell has a lower resistance, more current flows through it, generating more heat, and providing a positive feedback mechanism.

Under normal cell operation, internal heating might generate thermal gradients, such that the centre of the cell becomes hotter than the outer surface. The method described here allows users to simulate the effective charge transfer resistance of cells and quantify the errors brought about by a lumped thermal model, which is important especially in the case of high loads.

Acknowledgements

The authors would also like to acknowledge the EPSRC for funding of this work, through both a Career Acceleration Fellowship for Gregory Offer, in particular New Directions funding, award number EP/I00422X/1, and the FUTURE vehicle project, award number EP/I038586/1.

References

[1] V. Etacheri, R. Marom, R. Elazari, G. Salitra, D. Aurbach, Energy & Environmental Science 4 (2011) 3243.
[2] J.-S. Hong, H. Maleki, A. Al Hallaj, L. Redey, J.R. Selman, Journal of the Electrochemical Society 145 (1998) 1489.
[3] R. Spotnitz, J. Weaver, G. Yeduvaka, Journal of Power Sources 163 (2007) 1080.
[4] H.J. Ploehn, P. Ramadass, R.E. White, Journal of the Electrochemical Society 151 (2004) A456.
[5] P. Arora, R.E. White, M. Doyle, Journal of the Electrochemical Society 145 (1998) 3647.
[6] J. Vetter, P. Novák, M.R. Wagner, C. Veit, K.-C. Möller, J.O. Besenhard, M. Winter, M. Wohlfahrt-Mehrens, C. Vogler, a. Hammouche, Journal of Power Sources 147 (2005) 269.
[7] R. Spotnitz, J. Franklin, Journal of Power Sources 113 (2003) 81.
[8] D.P. Abraham, J. Liu, C.H. Chen, Y.E. Hyung, M. Stoll, N. Elsen, S. MacLaren, R. Twesten, R. Haasch, E. Sammann, I. Petrov, K. Amine, G. Henriksen, Journal of Power Sources 119-121 (2003) 511.
[9] D.P. Abraham, E.M. Reynolds, P.L. Schultz, a. N. Jansen, D.W. Dees, Journal of the Electrochemical Society 153 (2006) A1610.
[10] T.M. Bandhauer, S. Garimella, T.F. Fuller, Journal of the Electrochemical Society 158 (2011) R1.
[11] G. Guo, B. Long, B. Cheng, S. Zhou, P. Xu, B. Cao, Journal of Power Sources 195 (2010) 2393.
[12] R.P. Ramasamy, R.E. White, B.N. Popov, Journal of Power Sources 141 (2005) 298.
[13] A.J. Smith, H.M. Dahn, J.C. Burns, J.R. Dahn, Journal of the Electrochemical Society 159 (2012) A705.
[14] A. Jossen, Journal of Power Sources 154 (2006) 530.
[15] M. Fleckenstein, O. Bohlen, M.A. Roscher, B. Bäker, Journal of Power Sources 196 (2011) 4769.
[16] R.E. Gerver, J.P. Meyers, Journal of the Electrochemical Society 158 (2011) A835.
[17] G.-H. Kim, K. Smith, K.-J. Lee, S. Santhanagopalan, A. Pesaran, Journal of the Electrochemical Society 158 (2011) A955.
[18] H. Sun, X. Wang, B. Tossan, R. Dixon, Journal of Power Sources 206 (2012) 349.
[19] R. Spotnitz, Journal of Power Sources 113 (2003) 72.
[20] S. Chacko, Y.M. Chung, Journal of Power Sources 213 (2012) 296.
[21] M. Dubarry, N. Vuillaume, B.Y. Liaw, Journal of Power Sources 186 (2009) 500.
[22] G. Offer, V. Yufit, D. Howey, B. Wu, N. Brandon, Journal of Power Sources 206 (15 May 2012) 383–392.

[23] Y. Zheng, X. Han, L. Lu, J. Li, M. Ouyang, Journal of Power Sources 223 (2013) 136.
[24] C. Forgez, D. Vinh Do, G. Friedrich, M. Morcrette, C. Delacourt, Journal of Power Sources 195 (2010) 2961.
[25] D. Andre, M. Meiler, K. Steiner, C. Wimmer, T. Soczka-Guth, D.U. Sauer, Journal of Power Sources 196 (2011) 5334.
[26] D. Aurbach, M.D. Levi, E. Levi, H. Teller, B. Markovsky, G. Salitra, U. Heider, L. Heider, Journal of the Electrochemical Society 145 (1998) 3024.
[27] Y.M. Choi, S.I. Pyun, Solid State Ionics 99 (1997) 173.
[28] S. Rodrigues, N. Munichandraiah, A. Shukla, Journal of Solid State Electrochemistry 3 (1999) 397.
[29] T. Momma, M. Matsunaga, D. Mukoyama, T. Osaka, Journal of Power Sources 216 (2012) 304.
[30] J.P. Schmidt, D. Manka, D. Klotz, E. Ivers-Tiffée, Journal of Power Sources 196 (2011) 8140.
[31] E. Barsoukov, J.H. Jang, H. Lee, Journal of Power Sources 109 (2002) 313.
[32] S.C. Nagpure, R. Dinwiddie, S.S. Babu, G. Rizzoni, B. Bhushan, T. Frech, Journal of Power Sources 195 (2010) 872.
[33] A. Hensler, D. Wingert, C. Herold, J. Lutz, M. Thoben, Microelectronics Reliability 51 (2011) 1679.
[34] A. Eddahech, O. Briat, H. Henry, J.-Y. Delétage, E. Woirgard, J.-M. Vinassa, Microelectronics Reliability 51 (2011) 1968.
[35] N. Chaturvedi, R. Klein, J. Christensen, J. Ahmed, A. Kojic, IEEE Control Systems Magazine 49 (2010).
[36] J. Duan, B. Wei, R. Yang, C. Cai, J. Pan, Journal of Solid State Electrochemistry 16 (2011) 597.
[37] J. Gomez, R. Nelson, E.E. Kalu, M.H. Weatherspoon, J.P. Zheng, Journal of Power Sources 196 (2011) 4826.
[38] P. Suresh, A. Shukla, N. Munichandraiah, Journal of Applied Electrochemistry 32 (2002) 267.
[39] The Way to a Mobile Future Temperature and Climate Test Systems for Lithium-ion Batteries, Weiss Umwelttechnik Gmbh, 2010.
[40] R. Yazami, Y. Reynier, Journal of Power Sources 153 (2006) 312.
[41] Y. Reynier, R. Yazami, B. Fultz, Journal of Power Sources 119-121 (2003) 850.
[42] P.L. Moss, G. Au, E.J. Plichta, J.P. Zheng, Journal of the Electrochemical Society 155 (2008) A986.
[43] K. Kumaresan, G. Sikha, R.E. White, Journal of the Electrochemical Society 155 (2008) A164.
[44] Y. Ye, Y. Shi, N. Cai, J. Lee, X. He, Journal of Power Sources 199 (2011) 227.
[45] Y. Saito, K. Takano, K. Kanari, A. Negishi, K. Nozaki, K. Kato, Journal of Power Sources 97-98 (2001) 688.
[46] Y. Reynier, J. Graetz, T. Swan-Wood, P. Rez, R. Yazami, B. Fultz, Physical Review B 70 (2004) 1.
[47] A. Yamada, H. Koizumi, S.-I. Nishimura, N. Sonoyama, R. Kanno, M. Yonemura, T. Nakamura, Y. Kobayashi, Nature Materials 5 (2006) 357.
[48] V. Yufit, P. Shearing, R.W. Hamilton, P.D. Lee, M. Wu, N.P. Brandon, Electrochemistry Communications 13 (2011) 608.
[49] C.R. Pals, J. Newman, Journal of the Electrochemical Society 142 (1995) 3282.